Electron Field Emission Properties of Nanomaterials on Rough Silicon Rods

Hung-Chi Wu,[†] Tsung-Yen Tsai,[†] Fu-Hsuan Chu,[†] Nyan-Hwa Tai,[†] Heh-Nan Lin,[†] Hsin-Tien Chiu,[‡] and Chi-Young Lee*[,†,§]

Department of Materials Science and Engineering, National Tsing Hua University, Hsinchu 30013, Taiwan, Republic of China, Department of Applied Chemistry, National Chiao Tung University, Hsinchu, Taiwan 30010, Republic of China, and Center for Nanotechnology, Materials Science, and Microsystems, National Tsing Hua University, Hsinchu, Taiwan 30013, Republic of China

Received: September 4, 2009; Revised Manuscript Received: October 24, 2009

Highly porous, individually separated, and vertically aligned rough silicon rods (r-SiRs) were formed via a modified electroless metal deposition (EMD) approach. Despite inheriting the length of crowded silicon nanowires (NWs) obtained by the conventionally adopted EMD method, the r-SiRs are distributed sparsely, subsequently forming an excellent field emitter substrate. The electron field emission (EFE) of carbon nanotubes (CNTs) grown on r-SiRs can be turned on at $(E_0)_{CNTs/r\text{-}SiRs} = 2.3$ V/μm, yielding a high EFE current density, $(J_e)_{CNTs/r\text{-}SiR} = 3.7$ mA/cm^2 in an applied field of 5.1 V/μm. Additionally, a cactuslike structure consisting of zinc oxide NWs on r-SiRs can be turned on at 2.9 V/μm. The absence of a high-temperature or expensive photolithographic process makes r-SiRs a promising alternative as a silicon base field emitter substrate.

1. Introduction

One-dimensional (1D) nanostructures and 1D heterojunction structures, including nanowires (NWs), nanorods, nanotubes, and nanoneedles, have attracted considerable attention both in fundamental research and potential applications.[1−3] 1D nanostructured materials are regarded as ideal electric field emission sources owing to their high aspect ratio. Many 1D nanostructured materials, such as carbon nanotubes (CNTs),[4] zinc oxide (ZnO) NWs,[5] and silicon (Si) NWs,[6] as well as 1D heteronanostructure materials, such as tungsten nanothron grown on tungsten oxide nanowhiskers,[7] ZnO nanowires grown on CNTs,[8] and CNTs grown on SiNWs,[9] are considered highly promising field emitters. Various methods have been developed in recent decades for preparing silicon NWs used in nanoscale electronic and optoelectronic devices.[10−15] Among these, the electroless metal deposition (EMD) approach has attracted considerable attention owing to its relatively easy fabrication of well-aligned, single-crystalline, wafer-scale arrays of SiNWs.[15] Tzeng et al. took advantage of well-aligned SiNWs on a large-area single-crystal wafer by the conventionally adopted EMD process with its excellent properties of ultrananocrystalline diamond (UNCD), resulting in an extremely favorable electron field emissions (EFE) behavior.[16] However, the strong screening effect of crowded SiNWs degrades the performance of UNCD-coated SiNWs. According to theoretical predictions in a previous study, for nanowires with an aspect ratio exceeding 10, nanowires should be separated from each other by larger than 1 μm to suppress the "screening effect" induced by adjacent nanowires.[17] Typical SiNWs obtained by EMD method via the microelectrochemical redox reaction are aggregated and bundled SiNWs around the unreacted Si bulky centers (parts a−c of Figure 1).

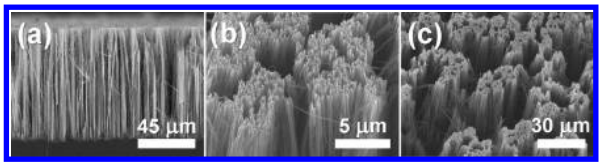

Figure 1. SEM images of (a) SiNWs, cross-sectional viewed image and and SiNWs at (b) high- and (c) low-magnification tilt-viewed images.

In this work, EMD SiNWs are adapted by anisotropic etching to lessen the population of SiNWs, resulting in individually separated rough silicon rods (r-SiRs) to form a substrate of EFE emitters.

2. Experimental Section

A. Preparation of SiNWs and r-SiRs. The SiNWs were obtained by conventional EMD method.[15] To fabricate r-SiRs, a modified EMD process was carried out. The SiNWs were dipped in HF-$AgNO_3$ mixture solution for 5 s to precipitate silver particles as electrodes and immersed in a temperature of 323 K HF-H_2O_2 alcoholic solutions to undergo an electrochemical redox reaction for 60 min. They were then cleaned with nitric acid and deionized water and then dried.

B. Synthesis of CNTs and ZnO NWs. The CNTs and ZnO NWs were synthesized on Si substrates (Si wafers, SiNWs and r-SiRs) by chemical vapor deposition.[18,19]

C. Characterizations. The as-synthesized samples were studied by micro-Raman spectroscopy (Lab Raman HR800, Jobin Yvon) using a He−Ne laser ($\lambda = 632.8$ nm) and X-ray diffraction (XRD, Bruker D8) using Cu Kα radiation. The surface morphology and crystallinity of the samples were observed using scanning electron microscopy (SEM, Jeol 6500F) and transmission electron microscopy (TEM, Jeol 2010), respectively. The chemical compositions of the products were analyzed using SEM/energy dispersive spectroscopy (EDS). CNTs and ZnO NWs were removed from the substrates by ultrasonication in ethanol. EFE measurements were made in a lab-built system at a base pressure under 3×10^{-6} Pa. The

* To whom correspondence should be addressed. E-mail: cylee@mx.nthu.edu.tw (C.-Y. L.).
† Department of Materials Science and Engineering, National Tsing Hua University.
‡ National Chiao Tung University.
§ Center for Nanotechnology, Materials Science, and Microsystems, National Tsing Hua University.

10.1021/jp908566q
Published on Web 11/03/2009

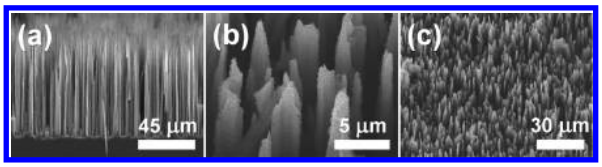

Figure 2. SEM images of (a) r-SiRs, cross-sectional viewed image and r-SiRs at (b) high- and (c) low-magnification tilt-viewed images.

sample was fixed on a stainless steel holder and used as a cathode. A rodlike molybdenum probe was the anode. A direct current voltage, swept from 0 to 1100 V in steps of 20 V, was applied to the sample. The dependence of the field emission current on the anode−cathode voltage (*IV* behavior) was recorded automatically with a Keithley 2410 source meter at intervals of 1 s.

3. Results and Discussion

Parts a−c of Figures 2 present cross-sectional and tilt-viewed SEM images of r-SiRs, as prepared by the modified EMD method. Massive rough silicon rods with lengths of around 90 μm and many small pores distributed all over them were formed distinguishably perpendicular to the substrate. In contrast with SiNWs prepared by conventional EMD method formed smooth surfaces shown in Figure 1, r-SiRs were rather extraordinary, with a rough, scraggly, and coarse appearance; the population of r-SiRs was significantly less dense than that of SiNWs. However, they all formed vertical arrays.

This unique morphology is formed as follows: the aggregated and bundled SiNWs around the unreacted Si rod centers on a silicon wafer was prepared by the conventionally adopted EMD method, as shown in Figure 1. Silver nanoparticles were then produced and aggregated among tips of SiNWs by dipping the SiNWs in $AgNO_3$ solution, as shown in Figure S1 of Supporting Information. Finally, the further redox reaction was performed in HF-H_2O_2 alcoholic solution. The second redox reaction, as achieved by anisotropic etching, occurred underneath the Ag nanoparticles, leading to oxidization and etching the silicon by HF and ultimately reducing and thinning the SiNW bundled arrays and forming r-SiRs.[20]

Two field emitters, CNTs and ZnO NWs, were grown on the free-standing, vertically aligned r-SiRs. CNTs on r-SiRs were prepared first. After 3 nm of iron film was deposited and CNTs were grown for 5 min, the substrates were covered with a black layer. Figure S3 in Supporting Information shows micro-Raman spectra of CNTs deposited on the substrates. Peaks around 1320 and 1590 cm^{-1} were consistent with typical Raman peaks of a CNT film.[21] Parts a−c of Figures 3 display SEM images of CNTs grown on various substrates, silicon wafer, SiNWs, and r-SiRs (inset displays the lower-magnified SEM images of CNTs grown on r-SiRs), respectively. Numerous entangled, threaded CNTs of around 100 μm in length were densely packed and vertically aligned on silicon wafer but were randomly oriented and curved on SiNWs and r-SiRs. CNTs covered only on the tips of SiNWs; however, the CNTs completely surrounded the silicon rods because they are separated from each other. Figure 3d presents a TEM image of CNTs attached to r-SiRs. Length of the CNTs was determined to be several micrometers, and small iron grains that acted as catalysts of CNTs growth[22] were encapsulated in the CNTs. The inset of Figure 3d presents the high resolution TEM image of multiwalled CNTs with a diameter of 20 nm, comprising about twenty concentric shells formed from well graphitized carbon sheets. Only a slight amount of the carbonaceous material is at the periphery of the CNTs.

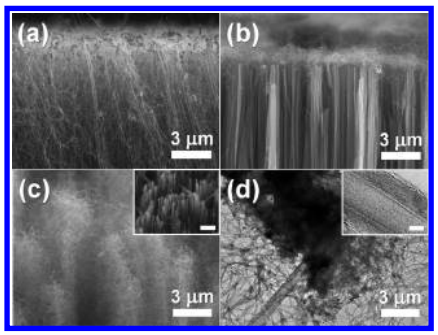

Figure 3. SEM images of CNTs grown on (a) silicon wafer, (b) SiNWs, and (c) r-SiRs (inset presents a low-magnification image of CNTs grown on r-SiRs, and the scale is 10 μm), (d) TEM image of CNTs attached to a r-SiR; inset presents high resolution TEM image of a CNT, and the scale is 5 nm.

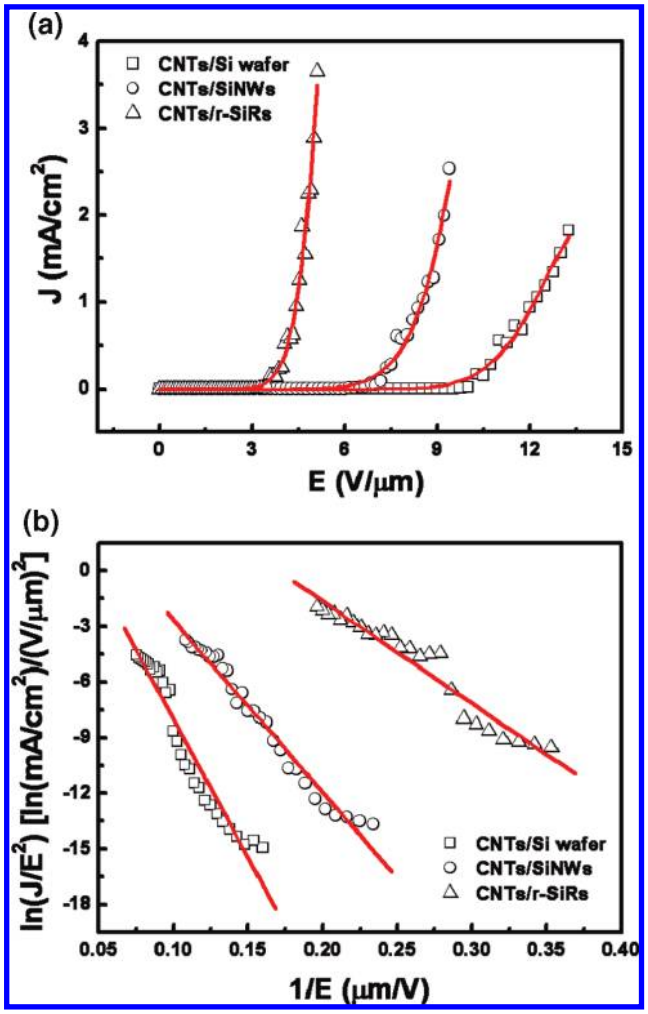

Figure 4. (a) Field emission current density as a function of applied electric field form CNTs grown on polished silicon wafer (square), SiNWs (circle), and r-SiRs (triangle). (b) F−N plot exhibits linear dependence and indicates that the emission is consistent by the F−N mechanism.

In addition to plotting the field emission current density as a function of the applied electric field (*JE*), Figure 4 displays the corresponding Fowler−Nordheim (F−N) plot[23] of catalytically grown CNT films on various substrates. Notably, the turn-on field (E_0) was estimated from the F−N plot of the *JE* curve as the intersection of two straight lines extrapolated from the low-field and high-field sections of the F−N plot.[16] In the F−N plots,

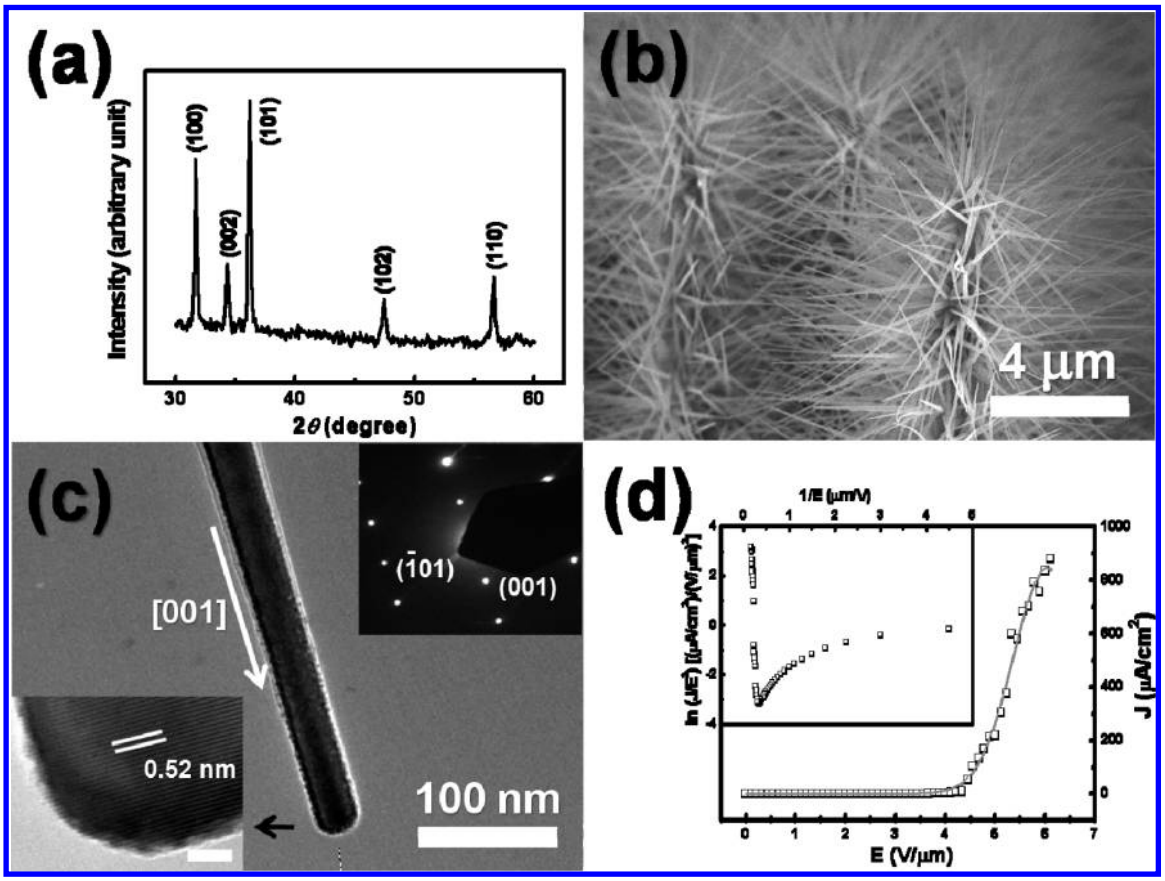

Figure 5. (a) XRD spectrum of ZnO NWs grown on r-SiRs. (b) Cross-sectional SEM image of ZnO/r-SiRs cactuslike heterojunction structures. (c) TEM image of a ZnO NW; upper inset presents a selected area electron diffraction pattern of the NW, and lower inset shows a high resolution TEM image of single NW, and the scale is 5 nm. (d) *JE* curve of EFE measurement from ZnO/r-SiRs cactuslike heterojunction structures, and the inset shows the corresponding F−N plot.

these straight lines indicate that the emission currents satisfy the conventional F−N equation

$$J = \frac{A\beta^2 E^2}{\Phi}\exp\left(-\frac{B\Phi^{3/2}}{\beta E}\right)$$

where J denotes the current density in A/m^2, E denotes the electric field in V/m, Φ represents the work function in eV, β is the field enhancement factor at a sharp point of the material, $A = 1.54 \times 10^{-6}$ A eV V^{-2}, $B = 6.83 \times 10^9$ eV$^{-3/2}$ V m^{-1}, and β is given by $\beta = \Phi^{3/2}/\Phi_e$ with the reported value for $\Phi = 5.0$ eV for CNTs where Φ_e refers to the effective work-function derived from the gradient o,f the F−N plot. CNT films vertically grown on a polished silicon wafer require a large turn-on field, $(E_0)_{CNTs/Si} = 6.7$ V/μm, to induce EFE and can reach a current density $(J_e)_{CNTs/Si} = 1.8$ mA/cm^2 in an applied field of $(E_a)_{CNTs/Si} = 13.2$ V/μm. The large turn-on field makes CNT films inappropriate for use as field emitters owing to the strong field screening effect. However, the EFE properties of CNTs randomly grown on SiNWs have improved such that a turn-on field, $(E_0)_{CNTs/SiNWs} = 4.3$ V/μm, can be reached and yield a current density $(J_e)_{CNTs/SiNWs} = 2.5$ mA/cm^2 in an applied field of $(E_a)_{CNTs/SiNWs} = 9.4$ V/μm. Although the SiNWs are a reliable substrate for UNCD-coated field emitters, the CNTs on SiNWs enhance the EFE property only slightly because of the large screening effect of the SiNWs substrates. However, CNTs grown on individual r-SiRs have a considerably satisfying EFE property. The turn-on field of CNTs/r-SiRs is $(E_0)_{CNTs/r\text{-}SiRs} = 2.3$ V/μm, and $(J_e)_{CNTs/r\text{-}SiRs} = 3.7$ mA/cm^2 can be reached at an applied field of $(E_a)_{CNTs/r\text{-}SiRs} = 5.1$ V/μm. Estimating the β factor for each specimen based on the F−N equation yields the value of CNTs grown on silicon wafers, SiNWs and r-SiRs, which are $(\beta)_{CNTs/Si} = 511$, $(\beta)_{CNTs/SiNWs} = 823$ and $(\beta)_{CNTs/r\text{-}SiRs} = 1384$, respectively. Si rods produced by the modified EMD method with a unique geometry are a more favorable basis for field emitters than SiNWs obtained by the conventional EMD method.

Next, the field emission property of the r-SiRs substrate was investigated further by using r-SiRs as a template to grow ZnO NWs via the surface-roughness-assisted method.[19] Cactuslike ZnO/r-SiRs heterojunction structures were formed. The crystal structure of the as-synthesized ZnO/r-SiRs was identified by XRD, as displayed in Figure 5a. The major peaks of the products appearing at around $2\theta = 31.8$, 34.4, and 36.2 were assigned to the (100), (002), and (101) planes of the hexagonal wurtzite ZnO phase, with lattice constants of $a = 0.325$ nm and $c = 0.521$ nm (JCPDS card no 36−1451). Figure 5b presents SEM cross-sectional image of ZnO grown on r-SiRs. Straight ZnO NWs with a length of around 5 μm were observed and randomly adhered to the surfaces of the silicon rods. The ZnO NWs grown on r-SiRs appeared to radiate out from them, forming cactuslike structures (Figure S4 of Supporting Information presents photographs of cacti, *Grusonia parishii*). All ZnO NWs were connected and grouped together at the tips of the r-SiRs, because of the surface roughness-assisted growth of these ZnO NWs. The microstructure of the ZnO NW was further analyzed using TEM. Figure 5c and its inset present the TEM image, HRTEM image, and the corresponding selected area electron diffraction (SAED) pattern, respectively. The TEM image reveals that the

end of the ZnO NW tip is round, with a curvature of around 30 nm. The SAED pattern in the inset indicates that the ZnO NWs have a wurtzite crystalline structure, with a preferential [001] orientation. The NW lattice spacing is approximately 0.52 nm, corresponding to the (001) crystal plane of the ZnO.

Figure 5d presents the *JE* and F−N plots of field emission properties about the cactuslike ZnO/r-SiRs heterostructures. The β factor was estimated using the reported work function of bulk ZnO, $\Phi_{ZnO} = 5.3$ eV. The ZnO NWs grown on r-SiRs with cactuslike nanostructures exhibits a superior field emission property to that of ZnO NWs on silicon wafers and SiNWs. The turn-on field of the ZnO/r-SiRs cactuslike nanostructure is $(E_0)_{ZnO/r\text{-}SiRs} = 2.9$ V/μm and $(J_e)_{ZnO/r\text{-}SiRs} =$ 900 μA/cm^2 can be reached at an applied field of (E_a)ZnO/r-SiRs = 8.6 V/μm. The β value of ZnO/r-SiRs cactuslike heterostructures is $(\beta)_{ZnO/r\text{-}SiRs} = 1311$.

Of 1D ZnO nanostructures, vertically aligned ZnO NWs grown on conductive gallium-doped Zn films have a turn-on field at 18 V/μm,[5] while novel nail-like and pencil-like nanostructures have a lower turn-on field of about 7 V/μm.[24] Nanorods grown using a solvothermal approach have differently sized tips and a lower turn-on field of 5.3 V/μm.[25] Pure and aligned in the *c* axis direction of the wurtzite structure ZnO nanoneedle arrays with tip diameter around 30 nm have a turn-on voltage at about 5.3 V/μm.[26] Additionally, ZnO nanoneedle structures grown using a selenium-controlled approach exhibited an ultrasharp tip at around 7 nm with a low turn-on field of 2.4 V/μm.[27] Comparing the EFE properties of these ZnO 1D structures demonstrates that the electron emission properties of the unique ZnO/r-SiRs cactuslike radiating heterojunction nanostructure are superior to those of NWs, nanonails, nanopencils, nanorods, and nanoneedles and that the former have a relatively low turn-on field similar to that of ultrasharp nanoneedles.

4. Conclusion

r-SiRs with a rough, scraggly, and an extremely coarse surface, standing distinguishably perpendicular to the substrate, were fabricated using a modified EMD method. Following a simple calculation, the population of r-SiRs is significantly less dense than that of SiNWs. CNTs grown on r-SiRs to form a heterojunction nano/microstructure have excellent EFE properties with a low turn-on field of 2.3 V/μm, a high β value, and a high current density. Moreover, ZnO NWs grown on r-SiRs to form a cactuslike structure exhibit excellent EFE properties and a low turn-on field of 2.9 V/μm. The excellent EFE performance of the heterojuction structures originates from not only the intrinsic properties of CNTs and ZnO NWs but also the unique geometry of separated individual r-SiRs. The r-SiRs fabrication procedure is an electroless self-alignment process without prepatterning. The approach is simple, inexpensive, and easily scalable. The formed rods are single-crystalline, vertically well aligned, with a large surface area, and silicon-based template. Given all of these advantages, rough silicon rods are recommended for use as silicon-based templates in electron emitter applications.

Acknowledgment. The authors would like to thank the National Science Council of the Republic of China, Taiwan, for financially supporting this research under Contract No. NSC-96-2113-M-007-021 and Mr. Daiv Freeman and Mr. Stan Shebs for providing the photographs of cacti.

Supporting Information Available: SEM image of silver nanoparticles capped on SiNWs and its corresponding SEM/EDS analysis, estimation pixels of SEM images of SiNWs and r-SiRs, micro-Raman spectra of CNTs grown on various silicon substrates, photographs of cacti, *Grusonia parishii*, and the similar ZnO/r-SiRs heteronanostructures. This material is available free of charge via the Internet at http://pubs.acs.org.

References and Notes

(1) Hu, J. T.; Ouyang, M.; Yang, P. D.; Lieber, C. M. *Nature* **1999**, *399*, 48.
(2) Huang, M. H.; Mao, S.; Feick, H.; Yan, H. Q.; Wu, Y. Y.; Kind, H.; Weber, E.; Russo, R.; Yang, P. D. *Science* **2001**, *292*, 1897.
(3) Cui, Y.; Wei, Q. Q.; Park, H. K.; Lieber, C. M. *Science* **2001**, *293*, 1289.
(4) Heer, W. A.; Chatelain, A.; Ugarte, D. *Science* **1995**, *270*, 1179.
(5) Tseng, Y. K.; Huang, C. J.; Cheng, H. M.; Lin, I. N.; Liu, K. S.; Chen, I. C. *Adv. Funct. Mater.* **2003**, *13*, 811.
(6) Riccitelli, R.; Di Carlo, A.; Fiori, A.; Orlanducci, S.; Terranova, M. L.; Santoni, A.; Fantoni, R.; Rufoloni, A.; Villacorta, F. J. *J. Appl. Phys.* **2007**, *102*, 054906.
(7) Baek, Y.; Song, Y.; Yong, K. *Adv. Mater.* **2006**, *18*, 3105.
(8) Yan, X. B.; Tay, B. K.; Miele, P. *Carbon* **2008**, *46*, 753.
(9) Liu, Y. M.; Fan, S. S. *Solid State Commun.* **2005**, *133*, 131.
(10) Zhang, R. Q.; Lifshitz, Y.; Lee, S. T. *Adv. Mater.* **2003**, *15*, 635.
(11) Holmes, J. D.; Johnston, K. P.; Doty, R. C.; Korgel, B. A. *Science* **2000**, *287*, 1471.
(12) Pan, H.; Lim, S.; Poh, C.; Sun, H.; Wu, X.; Feng, Y.; Lin, J. *Nanotechnology* **2005**, *16*, 417.
(13) Morales, A. M.; Lieber, C. M. *Science* **1998**, *279*, 208.
(14) Bauer, J.; Fleischer, F.; Breitenstein, O.; Schubert, L.; Werner, P.; Gosele, U.; Zacharias, M. *Appl. Phys. Lett.* **2007**, *90*, 012105.
(15) Peng, K. Q.; Wu, Y.; Fang, H.; Zhong, X. Y.; Xu, Y.; Zhu, J. *Angew. Chem., Int. Ed.* **2005**, *44*, 2737.
(16) Tzeng, Y. F.; Lee, Y. C.; Lee, C. Y.; Lin, I. N.; Chiu, H. T. *Appl. Phys. Lett.* **2007**, *91*, 063117.
(17) Givargizov, E. I.; Zhirnov, V. V.; Stepanova, A. N.; Rakova, E. V.; Kiselev, A. N.; Plekhanov, P. S. *Appl. Surf. Sci.* **1995**, *87*−*8*, 24.
(18) Chiu, C. C.; Tsai, T. Y.; Tai, N. H.; Lee, C. Y. *Surf. Coat. Technol.* **2006**, *200*, 3215.
(19) Ho, S. T.; Chen, K. C.; Chen, H. A.; Lin, H. Y.; Cheng, C. Y.; Lin, H. N. *Chem. Mater.* **2007**, *19*, 4083.
(20) The density ratio of SiNWs/r-SiRs estimated by the pixel of SiNWs and r-SiRs top view images is approximately 1.67. (Figure S1 of Supporting Information presents the detail of the estimation.).
(21) Eklund, P. C.; Holden, J. M.; Jishi, R. A. *Carbon* **1995**, *33*, 959.
(22) Lee, Y. T.; Park, J.; Choi, Y. S.; Ryu, H.; Lee, H. J. *J. Phys. Chem. B* **2002**, *106*, 7614.
(23) Fowler, R. H.; Nordheim, L. *Proc. R. Soc. London, Ser. A* **1928**, *119*, 173.
(24) Shen, G. Z.; Bando, Y.; Liu, B. D.; Golberg, D.; Lee, C. J. *Adv. Funct. Mater.* **2006**, *16*, 410.
(25) Dev, A.; Kar, S.; Chakrabarti, S.; Chaudhuri, S. *Nanotechnology* **2006**, *17*, 1533.
(26) Zhang, Z.; Yuan, H.; Zhou, J.; Liu, D.; Luo, S.; Miao, Y.; Gao, Y.; Wang, J.; Liu, L.; Song, L.; Xiang, Y.; Zhao, X.; Zhou, W.; Xie, S. *J. Phys. Chem. B* **2006**, *110*, 8566.
(27) Zhu, Y. W.; Zhang, H. Z.; Sun, X. C.; Feng, S. Q.; Xu, J.; Zhao, Q.; Xiang, B.; Wang, R. M.; Yu, D. P. *Appl. Phys. Lett.* **2003**, *83*, 144.

JP908566Q